Normal and Segmental Mode Dynamics of End-Functionalized Poly(propylene oxide) by Dielectric Relaxation Spectroscopy and Dynamic Mechanical Spectroscopy

Jovan Mijovic,* Mingyun Sun, and Yuefeng Han

Department of Chemical Engineering and Chemistry and The Herman F. Mark Polymer Research Institute, Polytechnic University, Six MetroTech Center, Brooklyn, New York 11201

Received February 22, 2002; Revised Manuscript Received May 2, 2002

ABSTRACT: An investigation was carried out of the normal and segmental dynamics of poly(propylene oxide) (PPO) chains with (1) symmetrical dipole inversion and (2) three-arm star configuration. PPO chains exhibit, in addition to the transverse dipole moment component ($\mu^{\perp}$) that gives rise to segmental (α) process, a persistent cumulative dipole moment along the chain contour ($\mu^{\parallel}$) that can be relaxed via the normal mode (α_N) process. Data were generated by broad-band dielectric relaxation spectroscopy (DRS) and dynamic mechanical spectroscopy (DMS), and the findings were contrasted. In comparison with the previous studies of PPO dynamics, our DRS and DMS results were generated over a broader range of frequency and temperature and on samples of a wider range of molecular architecture (molecular weight, type, and functionality of end group). Segmental and normal mode spectra were thermodielectrically simple (with the KWW β parameter of ca. 0.51). The average relaxation times for the segmental mode (τ_S) from DRS and DMS were in excellent agreement. A direct comparison of the normal mode relaxation times (τ_N) obtained from DRS and DMS data had to account for the longest viscoelastic relaxation time (τ_{N1DMS}) of the Rouse chain being one-half the longest dielectric relaxation time (τ_{N1DRS}) and twice the second dielectric normal mode relaxation time (τ_{N2DRS}), which is experimentally measured. We observed excellent agreement between (1) our DRS and DMS data, (2) our data and the results of other groups, and (3) our data and the prediction of the Rouse model for MW less than 12 000 g/mol. The molecular weight dependence of τ_{N1DMS} at 273 K is characterized by an exponent of 2, in perfect agreement with τ_{N2DRS}.

Introduction

In the past we have investigated the dynamics of a number of polymeric systems that undergo temporal evolution of structure as a result of various chemical and/or physical transformations, such as chemical cross-linking,[1−3] crystallization,[4] liquid crystallinity,[5] and phase separation.[6] Recently, we have initiated a program designed to add a new dimension to the studies of dipole dynamics in network-forming polymers. Of interest here is to investigate the dynamics of reactive systems where one of the components exhibits, in addition to the transverse dipole moment component ($\mu^{\perp}$) that gives rise to segmental α process, a persistent cumulative dipole moment along the chain contour ($\mu^{\parallel}$). This part of the dipole moment of the polymer molecule is present when the repeat unit lacks a plane of symmetry perpendicular to the chain contour, and it can be relaxed via the normal mode process, termed α_N. For a sequence of *n* units (without reversal of directional sense), the dipole vector must correlate with the displacement vector, implying a correspondence between dielectric and viscoelastic relaxations. The ultimate goal of our program is to provide an insight into the fundamental features *of* and the interplay *between* the segmental and normal mode dynamics in polymer networks of varying architecture.

In their pioneering studies in the 1960s, Stockmayer and co-workers first reported the presence of two dielectric dispersions in poly(propylene oxide),[7] or PPO, and termed chain molecules with a dipole component parallel to the chain contour *type A*.[8] It was not until the early 1980s, however, that the interest in the dynamics of type A polymers was revived, and a number of investigations were conducted on dilute, semidilute, and concentrated solutions of homopolymers that included poly(2,6-dichloro-1,4-phenylene oxide),[9] polychloroprene,[10] *cis*-polyisoprene (PI),[11−13] poly(phenoxyphosphazine),[14] and polylactones.[15] Studies of bulk polymers (*cis*-PI) were first reported by Adachi and Kotaka[16] and later by Boese and Kremer.[17] Watanabe et al. were the first to study *cis*-PI with the dipole sequence inverted (reversed) along the chain contour.[18]

The interest in more complex (than linear) polymers has a more recent origin. Watanabe et al.[19] and Schroeder and Roland[20] studied the normal mode process in *cis*-PI/polybutadiene (PB) blends. Karatasos et al.[21] studied poly(styrene-*b*-1,4-isoprene) diblock copolymers, while Floudas et al.[22] reported on the dynamics of PI in block copolymer/homopolymer blends. There are several excellent review articles in the literature that discuss the dynamics of nonreactive type A polymers.[23,24]

The work described herein focuses on a series of bi- and trifunctional poly(propylene oxides) (PPO) differing in molecular weight and the type of functional (reactive) end group. These PPO samples were selected for use as a type A containing reactive component in the ongoing investigation of network forming systems. A limited number of studies of PPO dynamics have been reported following Stockmayer's work. An early dielectric study of the segmental process in PPO as a function of temperature and pressure was reported by Williams.[25] Beevers et al.[26] conducted dielectric and Kerr effect relaxation measurements on entangled PPO and con-

* To whom correspondence should be addressed: e-mail jmijovic@poly.edu.

10.1021/ma020293b CCC: $22.00
Published on Web 06/07/2002

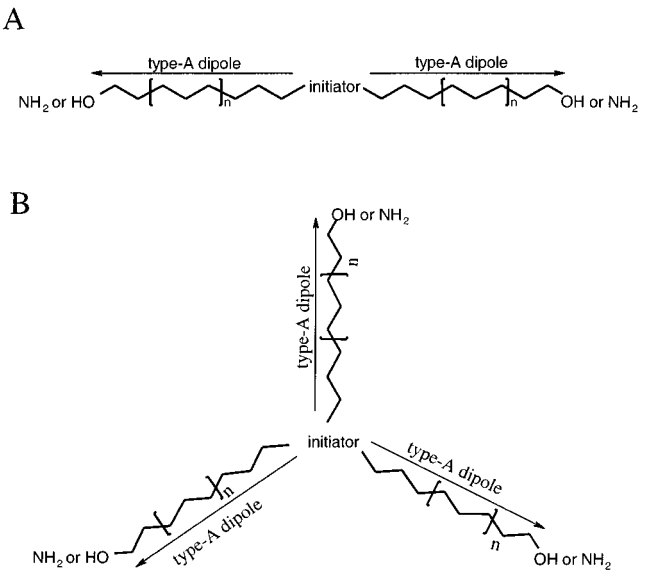

Figure 1. PPO architecture: (A) linear PPO chain with symmetrically inverted dipoles; (B) three-arm star PPO molecule. Note: the uninverted dipole sequence runs from the center to the end of each arm, and M_a denotes the molecular weight of each arm.

trasted the experimental results with the prediction of the reptation theory. Ngai, Schonhals, and Schlosser studied bulk poly(propylene glycol), PPG, and observed a molecular weight dependence of the average relaxation time for the normal mode that was stronger (the power of about 2.95) than predicted by the Rouse model.[27] They invoked hydrogen bonding and offered an explanation in terms of Ngai's coupling model, at odds with more recent studies that minimize the effect of hydrogen bonding on dynamics.[28,29] Nicolai and Floudas compared dielectric and viscoelastic response of PPO diols and triols and reported slower segmental and faster chain dynamics in dielectric measurements.[30] In an interesting recent study, Nicolai et al. reported that the dynamics of entangled and cross-linked PPO melts were identical (when the molecular weight for entanglements was equal to that between the cross-links).[31]

The aim of the present work was to gain a deeper insight into the nature of segmental and global processes in PPO and to set the stage for the forthcoming study of reactive networks. Novel information is generated and presented in comparison with the previous studies of PPO dynamics through our use of (1) wider temperature and frequency range (DRS measurements were conducted over 12 decades), thus obviating the need for master plots; (2) considerably greater molecular weight range, from unentangled to well-entangled (high MW PPOs are commercially unavailable and were synthesized in our lab); (3) varying number (two, three) and type (hydroxyl, amine) of functional (reactive) end group on the PPO chain; and (4) the measured values of zero shear viscosity.

Experimental Section

Materials. The two architectures of PPO molecules investigated in this study are shown in Figure 1: (A) linear PPO chains with symmetrical dipole inversion and (B) three-arm star PPO with each arm emanating from a central point and containing an uninverted dipole sequence. The characteristics of the samples investigated are summarized in Table 1. In the sample code used throughout the paper, the first letter defines

Table 1. PPO Samples Investigated[a]

code	trade name	M_n	M_a	M_w/M_n	source
BH0.425K	PPG_425	425	225.5		Bayer
BH0.725K	PPG_725	725	362.5		Bayer
BH2K	Acclaim	2000	1000	1.05	Bayer
BH4K	Acclaim	4000	2000	1.05	Bayer
BH8K	Acclaim	8000	4000	1.1	Bayer
BH12K	Acclaim	12000	6000	1.1	Bayer
TH3K	Acclaim	3000	1000	1.05	Bayer
TH6K	Acclaim	6000	2000	1.1	Bayer
BA2K	Jeffamine	2000	1000	1.05	Huntsman
TA3K	Jeffamine	3000	2000		Huntsman
TH284K		284000	94667	1.1	Own
TH398K		398000	132667	1.1	Own

[a] M_n is the number-average molecular weight (g/mol), and M_a (g/mol) is the molecular weight of the arm containing uninverted dipole sequence.

the *number* of functional groups (B = bifunctional, T = trifunctional); the second letter denotes the *type* of functional end group (H = hydroxyl, A = amine), and the number that follows defines the *molecular weight*. High molecular weight PPOs (MW > 10^5 g/mol) were synthesized and characterized in our lab according to the following procedure. Propylene oxide was polymerized at 30 °C in the presence of a catalyst—zinc hexacyanoferrate·$x$$ZnCl_2$·$y$Glyme·$z$$H_2O$ (III).[32] Fe^{3+} is obtained in preparations starting with a trivalent cyanide—iron complex, and this system is then used to conduct stereospecific polymerization that results in a three-arm polymer (Figure 1). The resulting PPO was semicrystalline, and the amorphous portion was extracted by dissolving in acetone at −20 °C. Higher (than 10^5) molecular weight was separated from the lower molecular weight fractions by dissolving the latter in isooctane at 0 °C. Fractionation was conducted by precipitation of decreasing MW fractions from the isooctane solution, induced by a stepwise decrease in temperature.[33] PPO was characterized by gel permeation chromatography—multiangle light scattering (GPC—MALS) system consisting of a Waters 510 pump, a 717 plus autoinjector, a Wyatt DAWN DSP multiangle laser light scattering photometer (Wyatt Technology, Santa Barbara, CA), and a Optilab DSP refractometer (Wyatt Technology). A three-column set consisting of 300 × 7.8 mm Styragel HR4, HR3, and HR1 was used to chromatograph the samples at room temperature. Chloroform was used as the mobile phase at a flow rate of 1 mL/min. Absolute molecular weights were determined using ASTRA software (Wyatt Technology). A specific refractive index increment (dn/dc) value of 0.025 mL/g was determined from the Bayer Acclaim BH12K sample and was then used for the high molecular weight samples. The following two molecular weight fractions (M_w, g/mol) were isolated (M_n, g/mol is given in parentheses): 284 000 (258 000) and 398 000 (358 000).

Techniques. *Dielectric Relaxation Spectroscopy* (*DRS*). Our facility combines commercial and custom-made instruments that include (1) Novocontrol's α high-resolution dielectric analyzer (3 μHz−10 MHz), (2) Solartron 1260 impedance/gain phase analyzer (10 μHz−32 MHz), (3) Hewlett-Packard 4284A precision LCR meter (20 Hz−1 MHz), (4) Hewlett-Packard 8752A network analyzer (300 kHz−1.3 GHz), and (5) Hewlett-Packard 4291B rf impedance analyzer (1 MHz−1.8 GHz). All instruments are interfaced to computers and equipped with heating/cooling controls, including Novocontrol's Novocool system custom-modified for measurements at low and high frequency. Further details have been given elsewhere.[34]

Dynamic Mechanical Spectroscopy (*DMS*). Experiments were conducted using a Rheometric Scientific's Advanced Rheometric Expansion System (ARES) rheometer. Measurements were performed in the frequency range from 0.001 to 100 rad/s and in the temperature range from 205 to 293 K. Parallel plate configuration was employed with a typical gap between the plates of ca. 1.5−2.0 mm. Strain values were adjusted from 0.2 to 25% for measurable torque in the linear viscoelastic range.

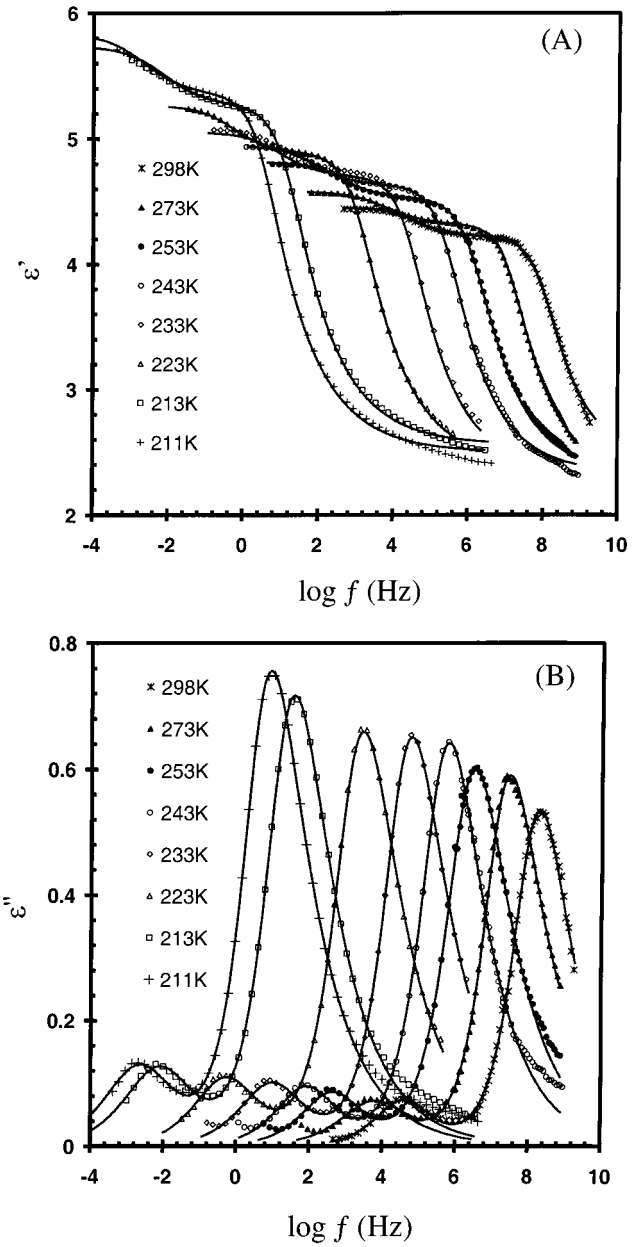

Figure 2. Dielectric permittivity (A) and dielectric loss (B) in the frequency domain (over 12 decades) with temperature as a parameter for BH12K.

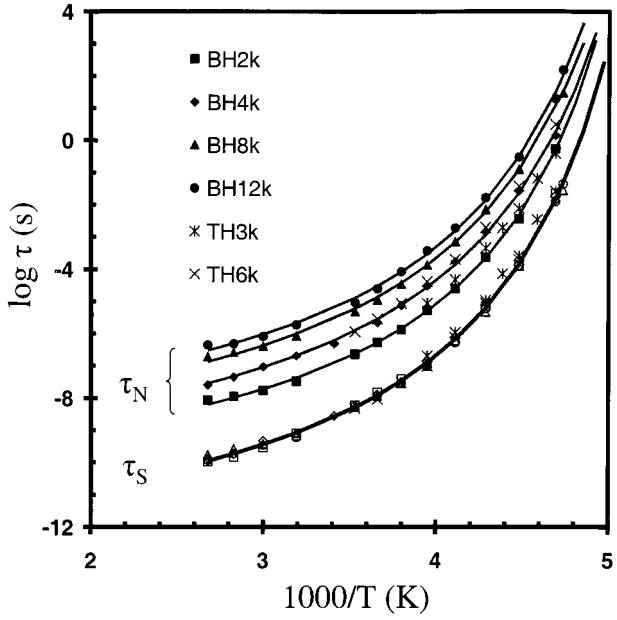

Figure 3. Temperature dependence of the average relaxation time for normal mode (solid symbols) and segmental mode (open symbols) with molecular weight as a parameter.

Results and Discussion

Dielectric permittivity and loss in the frequency domain[35] (over 12 decades) with temperature as a variable are shown in parts A and B of Figure 2, respectively, for a BH12K (bifunctional; hydroxyl terminated; MW = 12K) sample. Note how the temperature dependence of normal mode (lower frequency) and segmental mode (higher frequency) is beautifully discerned. The localized β process (not shown in this figure) was also observed. The solid lines in Figure 2 are fits to the Havriliak−Negami (HN) functional form.[36] The best results for the normal mode were obtained by setting the HN parameter $b = 1$, which reduces the HN equation to the Cole−Cole (CC) equation. With increasing temperature, the normal mode shifts to higher frequency and encroaches on the segmental mode (the α process). This phenomenon becomes more pronounced with decreasing molecular weight, and a physically meaningful separation of the two modes is not possible below the molecular weight of 1000 g/mol.

The temperature dependence of the relaxation time for segmental (τ_S) and normal (τ_N) mode (obtained from the HN fits) was examined next, and the results are plotted in Figure 3. An increase in the molecular weight slows down the normal mode but has no effect on the segmental mode. We note that only even normal modes are dielectrically active in our samples (with symmetrical dipole inversion) and that the contribution from the second normal mode dominates the response (i.e., $\tau_N = \tau_{N2}$). Moreover, in the chains with symmetrically inverted dipoles, the average relaxation time obtained from the loss peak is equal to the longest dielectric relaxation time.[37] The solid lines in Figure 3 are best fits to the Vogel−Fulcher−Tammann (VFT) equation; the corresponding VFT parameters are displayed in Table 2. Note that excellent fits of the segmental process were obtained with values of τ_{S0} below the attempt frequency of 10^{-14} s and that still lower values of τ_{N0} were needed for good VFT fits of the normal mode process. Interestingly, by setting the Vogel temperature (T_v) equal to the value obtained for the α process, we were able to generate excellent VFT fits for the normal mode relaxation. We also note that with decreasing temperature the α process slows down faster than the normal mode (but the two should not cross over; a theoretical explanation for that has been given by Ngai[38]). The faster slowdown of the segmental mode is more pronounced in the low molecular weight samples as exemplified in Figure 4. By plotting the ratio of τ_S and τ_N, we factor out the monomeric friction coefficient and the chain end effects.

Normalized loss spectra show that the segmental process remains thermodielectrically simple over a wide range of temperature, independent of the molecular weight; this is exemplified in Figure 5A for BH12K. Fits of the normalized spectra to the KWW functional form[39] yield a β_{KWW} of 0.51, a value typical of amorphous polymers. The temperature dependence of the relaxation time for the α process was also exploited to calculate the fragility. The calculated value of the Angell−Richert

Table 2. VFT Fit Parameters

	normal mode			segmental mode		
code	τ_0 (s^{-1})	E_a (eV)	T_v (K)	τ_0 (s^{-1})	E_a (eV)	T_v (K)
BH2K	7.74E−11	7.50E−02	1.75E+02	1.04E−12	7.95E−02	1.74E+02
BH4K	2.54E−10	8.18E−02	1.71E+02	8.93E−13	8.41E−02	1.72E+02
BH8K	1.20E−09	8.17E−02	1.72E+02	1.00E−12	8.23E−02	1.72E+02
BH12K	2.99E−09	7.91E−02	1.73E+02	1.05E−12	7.95E−02	1.74E+02
TH3K	8.26E−11	8.06E−02	1.72E+02	1.00E−12	8.58E−02	1.72E+02
TH6K	3.33E−10	7.84E−02	1.74E+02	1.00E−12	8.13E−02	1.74E+02

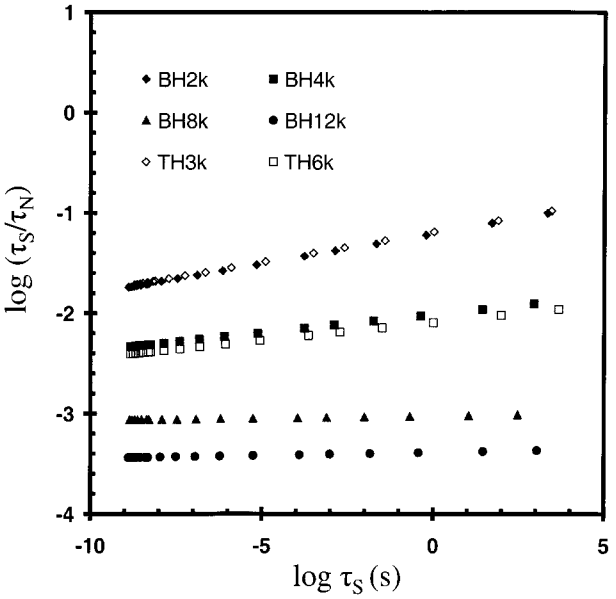

Figure 4. A plot of the ratio of relaxation times for segmental and normal mode scaled by the logarithm of the segmental relaxation time, with molecular weight as a parameter.

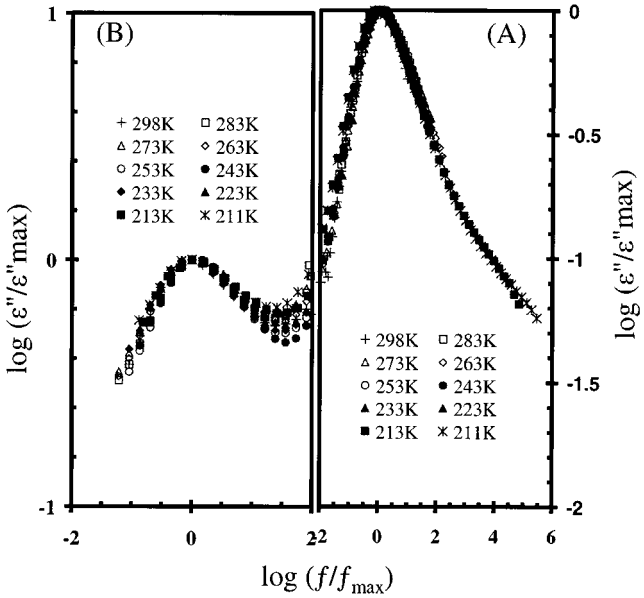

Figure 5. Normalized dielectric loss spectra for BH12K. Note that both segmental mode (A) and normal mode (B) process are thermodielectrically simple.

fragility index,[40] $F_{1/2} = 0.64$, places our materials on the fragile end of the strong−fragile classification scheme. The normal mode process is also thermodielectrically simple, as shown in the inset of Figure 5B. Normal mode distribution is characterized by a β_{KWW} of 0.50 for all molecular weights between 2000 and 12 000 g/mol. Normal mode distribution is usually narrower than the segmental mode, but that was not the case here. The

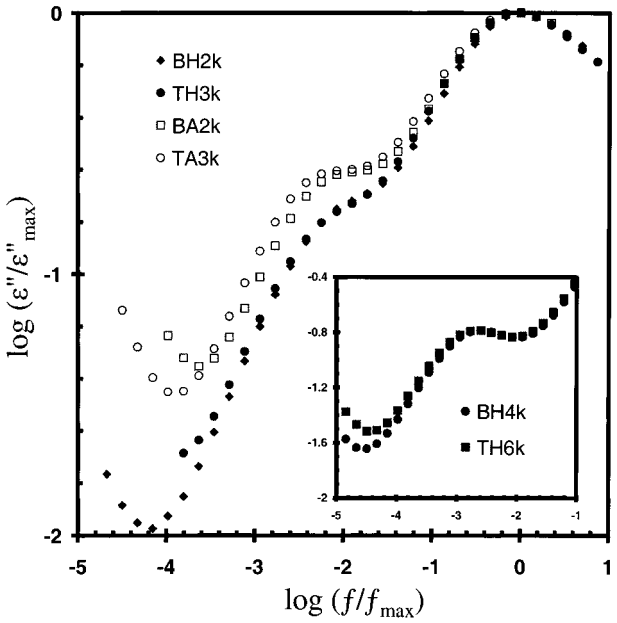

Figure 6. Normalized dielectric loss for diols, diamines, triols, and triamines with the same arm length (M_a). Note a broader spectrum in triol vs diol and triamine vs diamine with the same M_a of 1000 g/mol. The inset shows an analogous result for M_a of 2000 g/mol.

absence of change in the (dielectric) normal mode distribution below and above the molecular weight for entanglements is in agreement with the findings of Watanabe and his colleagues[25] but at odds with some other reports.[41,42]

We next examined the dependence of the relaxation time for the normal mode process on M_a—the molecular weight of the arm that contains the uninverted dipole sequence. Results were generated for a series of diols and triols with M_a from 2000 to 6000 g/mol (MW from 4000 to 12 000 g/mol). The calculated relaxation time scales with M_a to the power of 2, in agreement with the Rouse model.

Of further interest was to confirm that the dielectric normal mode process scales with M_a and not the overall molecular weight, MW. To that end, we have directly compared samples of different overall molecular weight (MW) but same uninverted dipole arm length (M_a). In Figure 6 we show normalized dielectric loss for a series of PPO samples with the same arm length of $M_a = 1000$ g /mol and different overall molecular weight (including diol and diamine with MW = 2000 g/mol and triol and triamine with MW = 3000 g/mol). Normalization is performed with respect to the segmental process, and it is observed that the general characteristics of the normal mode process in the samples of different MW but same M_a are quite similar. Slight discrepancies are expected considering different sample sources and inherent microstructural defects, such as a few (unavoidable) head-to-head and/or tail-to-tail links. Further

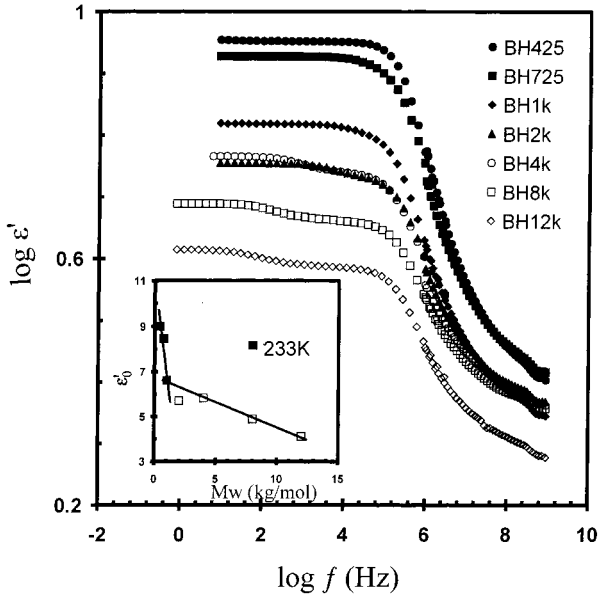

Figure 7. Dielectric permittivity in the frequency domain (over 12 decades) at 233 K, with molecular weight as a parameter. Inset: note that the limiting low-frequency dielectric permittivity decreases with increasing molecular weight and that an abrupt change occurs above 2000 g/mol.

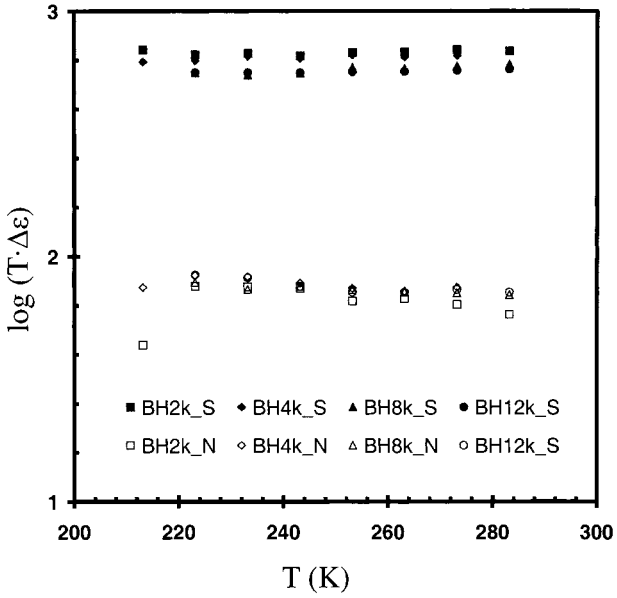

Figure 8. Temperature-corrected dielectric strength of the normal mode and segmental mode as a function of temperature. Open and filled symbols are for normal and segmental mode, respectively.

confirmation comes from the normalized loss data for the uninverted dipole arm of $M_a = 2000$ g/mol, shown in the inset in Figure 6, where a diol (MW = 4000 g/mol) and a triol (MW = 6000 g/mol) obtained from the same source are compared. Again, the observed agreement between the two spectra is excellent. We therefore conclude that our dielectric results for symmetrically inverted linear and three-arm star PPOs reflect the normal mode process associated with M_a, i.e., the molecular weight of the arm that contains the uninverted dipole sequence.

Next, we examined the dielectric relaxation strength of the segmental ($\Delta\epsilon_S$) and the normal mode ($\Delta\epsilon_N$) process. $\Delta\epsilon$ is an important materials characteristic because it depends on the chemical structure and molecular architecture. Relaxation strength is defined as $\Delta\epsilon = \epsilon'_0 - \epsilon'_\infty$, where ϵ'_0 and ϵ'_∞ represent the limiting low- and high-frequency dielectric permittivity for a given process, respectively, and is proportional to the concentration of dipoles and the mean-squared dipole moment per molecule. $\Delta\epsilon$ was obtained from the HN fits of dielectric permittivity in the frequency domain with molecular weight as a parameter; an example of such data at 233 K is shown in Figure 7. As shown in the inset in Figure 7, there is a critical point around 2000 g/mol, above which ϵ'_0 decreases much more slowly. The dielectric relaxation strength of the segmental process ($\Delta\epsilon_S$) decreases with increasing molecular weight and increasing temperature. The dielectric relaxation strength of the normal mode process ($\Delta\epsilon_N$) is a very weak (decreasing) function of temperature. Note also that the limiting low-frequency dielectric permittivity is a strong function of the molecular weight. The temperature corrected dielectric strength of the α process ($T\Delta\epsilon_S$) is independent of temperature as seen in Figure 8. This finding is in agreement with reported results.[30]

The results of dynamic mechanical spectroscopy (DMS) are considered next. Storage modulus (G') and loss modulus (G'') in the frequency domain for BH12K measured at 211 K are shown in Figure 9. Segmental

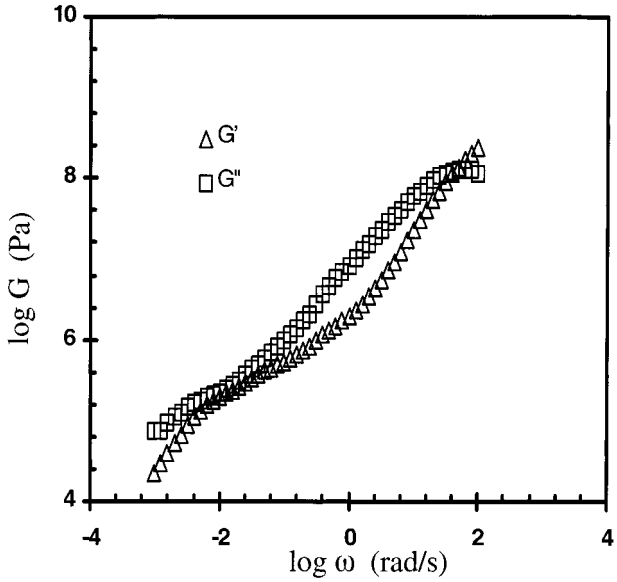

Figure 9. Storage modulus (G') and loss modulus (G'') in the frequency domain for BH12K at 211 K. Note how segmental and terminal processes are clearly discernible.

and terminal relaxations are clearly discerned, and an analogous observation was made for all samples of molecular weight equal to or greater than 2000 g/mol. Figure 10 shows storage modulus in the frequency domain measured at 211 K, with molecular weight as a parameter. The segmental process was found to be a weak function of molecular weight, and in that respect our results parallel those of others.[43] A small horizontal shift to lower frequency, with BH12K as a reference, was effected in Figure 10 in order to coalesce the data in the segmental range and show more clearly the molecular weight dependence in the terminal zone. The plateau modulus (G_N) was determined from Figure 10 by taking the value of the onset of transition from segmental to terminal mode in the sample with molecular weight of 4000 g/mol. The thus obtained value of 7×10^5 Pa was used in the subsequent calculations. A

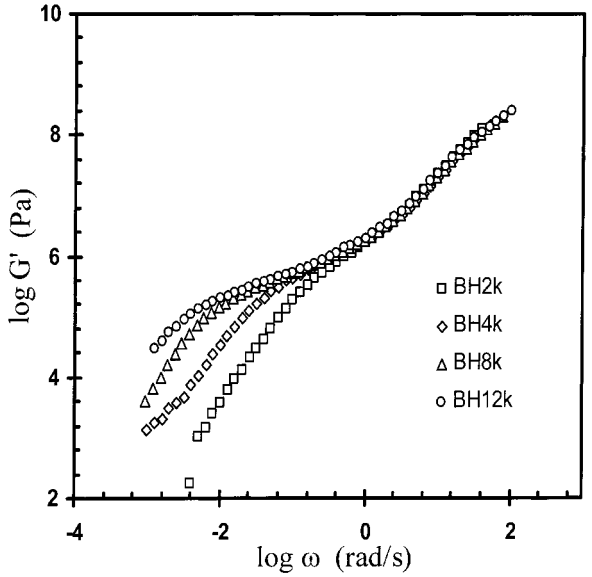

Figure 10. Storage modulus (G') in the frequency domain at 211 K with molecular weight as a parameter. Note: BH12K was used as a reference, and a small horizontal shift was effected to coalesce the data in the segmental relaxation range.

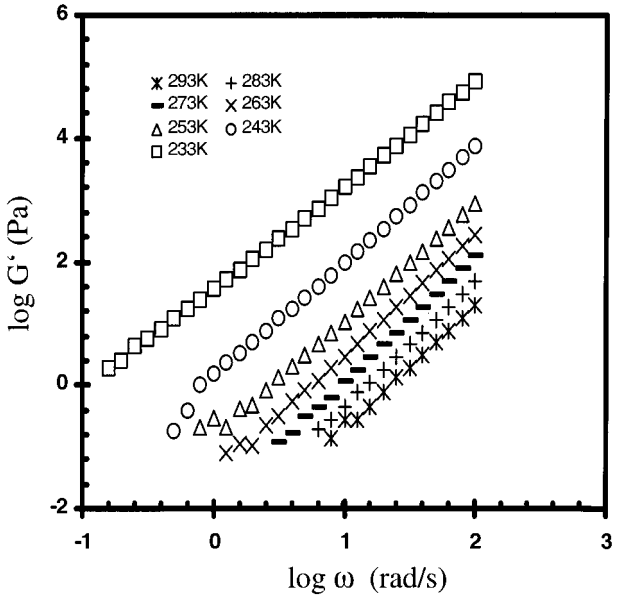

Figure 11. Storage modulus (G') in the frequency domain in the terminal relaxation range for BH4K, with temperature as a parameter.

closer examination of the data in the terminal relaxation zone at various temperatures reveals that G'' varies with frequency to the power of 1, independent of temperature, while the G' frequency dependence is temperature-sensitive. An example of the G' temperature dependence is shown in Figure 11, and the results obtained for different molecular weights are summarized in Table 3. Note how the power law exponent decreases from the value of 2 at 323 K to about 1.5 at 233 K. The zero-shear viscosity (η_0) was extracted directly from the data by averaging the low shear rate values of η. Identical results were obtained by calculating the zero-shear viscosity from $\eta_0 = \lim\{G''(\omega)/\omega\}$ as $\omega \rightarrow 0$. In Figure 12 we show a log−log plot of η_0 as a function of molecular weight. The first two linear portions, seen in this plot, with exponents of one and two, were characteristic for the MW range from 2000

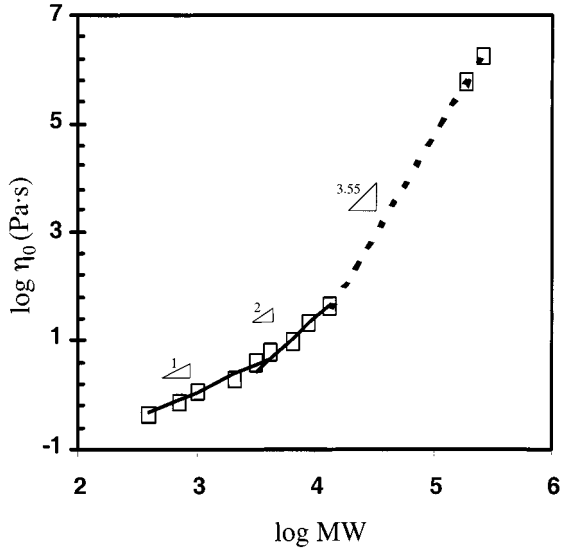

Figure 12. Zero-shear viscosity as a function of the overall molecular weight at 273 K.

Table 3. Exponential Dependence of the G' vs Frequency for Different Molecular Weights at Terminal Zone

code	293 K	283 K	273 K	263 K	253 K	243 K	233 K
BH2K		2.11	2.06	2	2.01	1.95	1.8
BH4K	2.03	2.01	2.05	1.95	1.9	1.85	1.62
BH8K	1.95	1.95	1.89	1.87	1.81	1.64	1.51
BH12K	1.93	1.78	1.84	1.76	1.55	1.48	1.57

to 12 000 g/mol, at all temperatures. The change in the slope from one to two denotes the onset of entanglements and is observed at a molecular weight between 3000 and 4000 g/mol, in agreement with previous reports.[30,31] Note that the data for diols and triols fall on the same line. The terminal time and viscosity of well-entangled monodisperse star-branched polymers are known to depend only on M_a and not the number of arms,[44] and our results follow that trend too. To test the response of higher MW samples, well above 12 000 g/mol, we have conducted an elaborate program of synthesis, fractionation, purification, and characterization, described in the Experimental Section. Two such samples, with M_w of 284 000 and 398 000 g/mol, were successfully prepared and tested: the resulting points are included in Figure 12. A dashed line with the slope of 3.55 was obtained. Although only two high MW samples were tested, there is no doubt that the exponent increases well above two, but a further systematic study of additional high MW samples is needed in order to establish its exact value.

Normalized loss spectra for the segmental process in BH12K are shown in Figure 13: the process is thermorheologically complex, as the spectra become broader with decreasing temperature. This is apparent from the low-frequency side of Figure 13. (The high-frequency side DMS data are less accurate further from the peak.) We note that this behavior is in contrast with the DRS results (shown in the inset in Figure 13 for the same temperature range), which are characterized by thermodielectric simplicity and a KWW β parameter of 0.51.

We next focus attention on a comparative analysis of DRS and DMS results. Notwithstanding the fact that DRS and DMS results reflect the same chain motion, a direct comparison of dielectric and viscoelastic relaxation function must account for the difference in the physics that underlies the material's response to electric

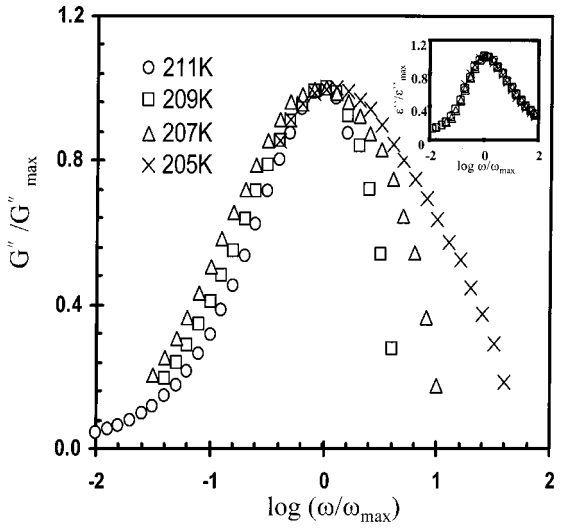

Figure 13. Normalized DMS loss spectra for BH12K. Inset: normalized DRS loss spectra.

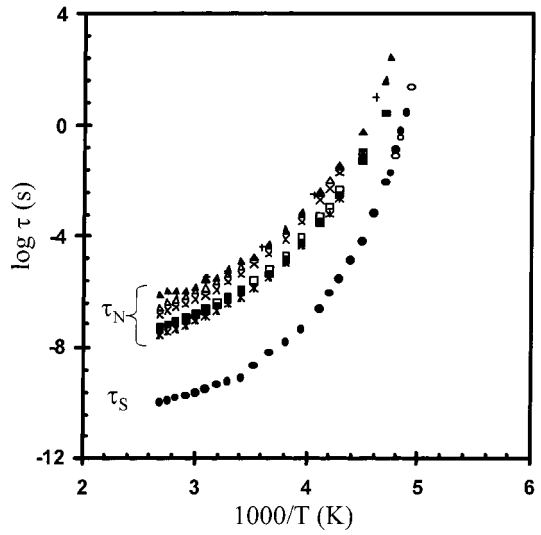

Figure 14. Average DMS and DRS relaxation time for segmental (τ_S) time and normal (τ_N) process as a function of reciprocal temperature. Code: filled circles, τ_{SDRS}; open circles, τ_{SDMS}; filled squares, τ_{NDRS} for BH4K; open squares, τ_{NDMS} for BH4K; stars, Rouse model for BH4K; filled triangles, τ_{NDRS} for BH12K; open triangles, τ_{NDMS} for BH12K; X, Rouse model for BH12K; crosses, data from ref 30.

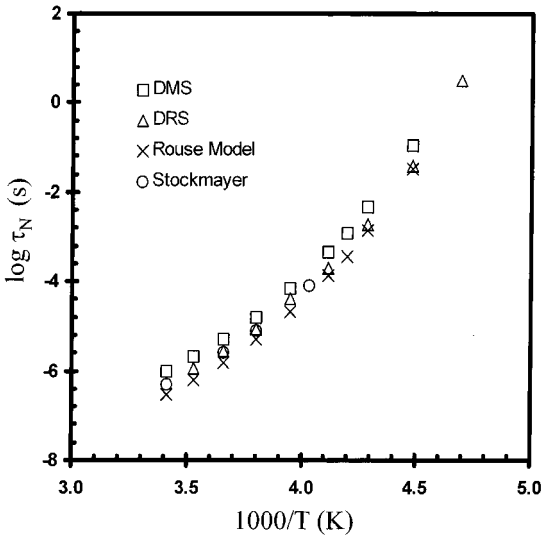

Figure 15. Average relaxation time for the normal mode process of a three-arm star PPO (TH6K) as a function of reciprocal temperature.

and mechanical fields. Specifically this is reflected in the fact that the changes in the autocorrelation function that defines dielectric relaxation are detected as the difference in the orientational correlation at two different times, while the viscoelastic orientation function detects orientational anisotropy at the same time but at two different positions. This is an important distinction that has received considerable attention in a series of studies by Watanabe and his colleagues in the past 10 years.[24] The key point is that the calculation of G^* from ϵ^*, and vice versa, is possible only when the details of the relaxation mechanism are known. For example, for the case of pure reptation the longest relaxation time is the same for dielectric and viscoelastic correlation functions, and the normalized viscoelastic, $\mu(t)$, and dielectric, $\phi(t)$, relaxation functions are related by $\mu(t) = \phi(t)$, while the inclusion of dynamic tube dilation modes yields the following relation:[45] $\mu(t) = [\phi(t)]^2$. Our goal here is not to be comprehensive but simply to contrast the relaxation time and the normalized relaxation function obtained from DRS and DMS measurements. Figure 14 is a composite plot of segmental and normal mode relaxation time for linear PPOs with symmetrically inverted dipoles, obtained from DRS and DMS results, as a function of temperature and molecular weight. A sample code is given in the caption. The average relaxation time for the segmental mode from DRS and DMS data was determined from $\tau_S = 1/\omega_{max} = {}^1/_2\pi f_{max}$. The average relaxation time for the normal mode from DRS data was obtained from the HN fits (that value coincides with $\tau_N = 1/\omega_{max}$, because of the symmetry of the dielectric normal mode spectrum). The average DMS normal mode relaxation time, τ_N, was calculated from[46]

$$\tau_N \equiv \frac{\eta_0}{G_N} = \frac{\sum_p \tau_{G,p} h_p}{\sum_p h_p}$$

where $\tau_{G,p}$ and h_p are the relaxation time and the intensity for the pth viscoelastic relaxation mode, and η_0 and G_N are as previously defined. To afford a direct comparison of τ_N obtained from DRS and DMS data, we had to multiply the DRS τ_N by two. This is because the longest viscoelastic relaxation time (τ_{N1DMS}) of the Rouse chain is one-half the longest dielectric relaxation time (τ_{N1DRS}) and twice the second dielectric normal mode (τ_{N2DRS}), which is experimentally measured in samples with symmetrically inverted dipoles. Hence, $\tau_{N1DMS} = {}^1/_2\tau_{N1DRS} = 2\tau_{N2DRS}$. Figure 14 is quite informative, and several points are worth making. We note the excellent agreement between (1) our DRS and DMS data, (2) our data and Floudas' and Nicolai's data[30] for BH12K, and (3) our data and the prediction of the Rouse model. Similar findings are recorded for three-arm star PPOs, as exemplified in Figure 15. Note the excellent agreement of our data with Stockmayer's data[47] for TH6K (M_a = 2K) and with the prediction of the Rouse model. The molecular weight (for MW < 12K) dependence of the longest relaxation time at 273 K is characterized by an exponent of 2, in agreement with the DRS data (Figure 16). In Figure 17 we show a comparison of normalized dielectric ($\epsilon''/\Delta\epsilon_N$) and viscoelastic ($G''/G_N$)

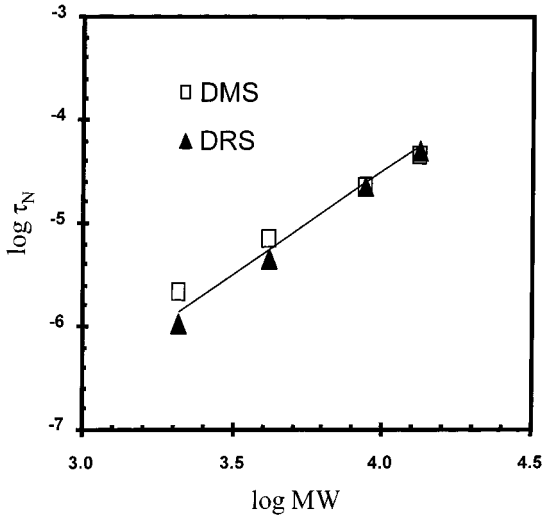

Figure 16. Average DRS and DMS relaxation time for the normal mode process as a function of the overall molecular weight.

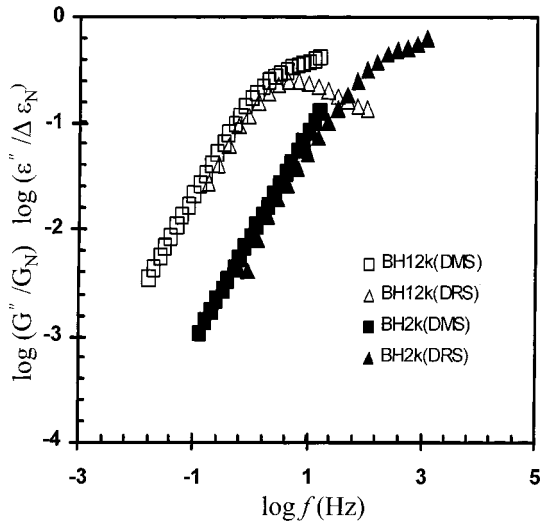

Figure 17. A comparison of the reduced dielectric ($\epsilon''/\Delta\epsilon_N$) and viscoelastic ($G''/G_N$) losses in the frequency domain for BH2K and BH12K.

losses. Figure 17 contains data for two samples: BH12K and BH4K. The ϵ'' data are normalized by the dielectric relaxation strength for the normal mode process ($\Delta\epsilon_N$) and the G'' data by the entanglement plateau modulus (G_N). Note that the reduced dielectric and viscoelastic losses coincide for each molecular weight. No attempts were made to deconvolute the segmental process from the viscoelastic data, and that accounts for the observed divergence at higher frequency. Of considerable interest, of course, would be to compare the normalized dielectric and viscoelastic relaxation function for higher MW PPOs, and we plan to report on that in a forthcoming publication.

Conclusions

We have completed an investigation of relaxation dynamics of poly(propylene oxide) (PPO) chains of varying molecular weight and molecular architecture. Experimental results were generated over a wide range of frequency and temperature using dielectric relaxation spectroscopy (DRS) and dynamic mechanical spectroscopy (DMS). The principal conclusions are as follows. The temperature dependence of the average relaxation time for the segmental and normal mode process is of the VFT type, the latter being a function of molecular weight. The segmental process is thermorheologically complex but thermodielectrically simple, with a KWW β of 0.51. Interestingly, the normal mode process also exhibits thermodielectric simplicity and is characterized by a KWW β of 0.5, a somewhat lower value (hence broader spectrum) than found in other polymers. The relaxation time for the normal mode process scales with M_a—the molecular weight of the arm that contains an uninverted dipole sequence. For $M_a \leq 6000$ g/mol, the DRS and DMS data agree very well with the prediction of the Rouse model, and the normalized dielectric ($\epsilon''/\Delta\epsilon_N$) and viscoelastic ($G''/G_N$) losses coincide. The plot of η_0 as a function of molecular weight has three linear parts. The first two, with exponents of one and two, were characteristic for the MW range from 2000 to 12 000 g/mol, at all temperatures. The change in the slope from one to two denotes the onset of entanglements and is observed at a molecular weight between 3000 and 4000 g/mol. For high MW samples (284 000 and 398 000 g/mol) the exponent increases well above 2 (a dashed line with the slope of 3.55 is drawn through these points as the guide for the eye in the text), but a further systematic study of additional high MW samples is needed in order to establish its exact value.

Acknowledgment. This material is based on work supported by National Science Foundation under Grants DMR-0101182 and DMR-9975592 (instrumentation grant).

References and Notes

(1) Andjelic, S.; Fitz, B.; Mijovic, J. *Macromolecules* **1997**, *30*, 5239.
(2) Fitz, B.; Mijovic, J. *Macromolecules* **1999**, *32*, 4134.
(3) Fitz, B.; Mijovic, J. *Macromolecules* **2000**, *33*, 887.
(4) Sy, J. W.; Mijovic, J. *Macromolecules* **2000**, *33*, 933.
(5) Mijovic, J.; Sy, J. W. *Macromolecules* **2000**, *33*, 6620.
(6) Mijovic, J.; Shen, M.; Sy, J. W.; Mondragon, I. *Macromolecules* **2000**, *33*, 5235.
(7) Baur, M. E.; Stockmayer, W. H. *J. Chem. Phys.* **1965**, *43*, 4319.
(8) Stockmayer, W. H. *Pure Appl. Chem.* **1967**, *15*, 539.
(9) Adachi, K.; Kotaka, T. *Macromolecules* **1983**, *16*, 1936.
(10) Adachi, K.; Kotaka, T. *Macromolecules* **1985**, *18*, 295.
(11) (a) Adachi, K.; Kotaka, T. *Macromolecules* **1987**, *20*, 2018. (b) Adachi, K.; Kotaka, T. *Macromolecules* **1988**, *21*, 157.
(12) Patel, S. S.; Takahashi, K. M. *Macromolecules* **1992**, *25*, 4382.
(13) Watanabe, H.; Yamada, H.; Urakawa, O. *Macromolecules* **1995**, *28*, 6443.
(14) Uzaki, S.; Adachi, K.; Kotaka, T. *Macromoleclues* **1988**, *21*, 153.
(15) (a) Baysal, M. B.; Stockmayer, W. H. *Macromolecules* **1994**, *27*, 7429. (b) Urakawa, O.; Adachi, K.; Kotaka, T.; Takemoto, Y.; Yasuda, H. *Macromolecules* **1994**, *27*, 7410.
(16) (a) Adachi, K.; Kotaka, T. *Macromolecules* **1984**, *17*, 120. (b) Adachi, K.; Kotaka, T. *Macromolecules* **1985**, *18*, 466.
(17) Boese, D.; Kremer, F. *Macromolecules* **1990**, *23*, 829.
(18) (a) Watanabe, H.; Urakawa, O.; Kotaka, T. *Macromolecules* **1993**, *26*, 5073. Watanabe, H.; Urakawa, O.; Kotaka, T. *Macromolecules* **1994**, *27*, 3525.
(19) Watanabe, H.; Urakawa, O.; Yamada, H.; Yao, M.-L. *Macromolecules* **1996**, *29*, 755.
(20) Schroeder, M. J.; Roland, C. M. *Macromolecules* **1999**, *32*, 2000.
(21) Karatasos, K.; Anastasiadis, S. H.; Floudas, G.; Fytas, G.; Pispas, S.; Hadjichristidis, N.; Pakula, T. *Macromolecules* **1996**, *29*, 1326.
(22) Floudas, G.; Meramveliotaki, K.; Hadjichristidis, N. *Macromolecules* **1999**, *32*, 7496.
(23) (a) Adachi, K.; Kotaka, T. *Prog. Polym. Sci.* **1993**, *18*, 585. (b) Adachi, K. In *Dielectric Spectroscopy of Polymeric Materi-*

als; Runt, J. P., Fitzgerald, J. J., Eds.; American Chemical Society: Washington, DC, 1997; Chapter 9, pp 261−282.
(24) (a) Watanabe, H. *Prog. Polym. Sci.* **1999**, *24*, 1253. (b) Watanabe, H. *Macromol. Rapid Commun.* **2001**, *22*, 127.
(25) Williams, G. *Trans. Faraday Soc.* **1965**, *61*, 1564.
(26) Beevers, M. S.; Elliott, D. A.; Williams, G. *Polymer* **1980**, *21*, 13.
(27) Ngai, K. L.; Schonhals, A.; Schlosser, E. *Macromolecules* **1992**, *25*, 4915.
(28) Randrianantoandro, H.; Nicolai, T. *Macromolecules* **1997**, *30*, 2460.
(29) Hayakawa, T.; Adachi, K. *Polymer* **2001**, *42*, 1725.
(30) Nicolai, T.; Floudas, G. *Macromolecules* **1998**, *31*, 2578.
(31) Nicolai, T.; Prochazka, F.; Durand, D. *Phys. Rev. Lett.* **1999**, *82*, 863.
(32) Herold, R. J. *Macromol. Synth.* **1974**, *5*, 9.
(33) Allen, G.; Booth, C.; Jones, M. N. *Polymer* **1964**, *5*, 257.
(34) Fitz, B.; Andjelic, S.; Mijovic, J. *Macromolecules* **1997**, *30*, 5227. (b) Mijovic, J.; Miura, N.; Monetta, T.; Duan, Y. *Polym. News* **2001**, *26*, 251.
(35) The fundamental aspects of DRS, theoretical and experimental, will not be discussed here. For recent reviews the interested reader is referred to: (a) Williams, G. Dielectric relaxation spectroscopy of amorphous polymer systems: the modern approaches. In *Keynote Lectures in Selected Topics of Polymer Science*; Riande, E., Ed.; CSIC: Madrid, 1997; Chapter 1, pp 1−40. (b) Williams, G. Theory of dielectric properties. In *Dielectric Spectroscopy of Polymeric Materials*; Runt, J. P., Fitzgerald, J. J., Eds.; American Chemical Society: Washington, DC, 1997; Chapter 1, pp 3−65.
(36) Havriliak, S. Jr.; Negami, S. *Polymer* **1967**, *8*, 161.
(37) Yoshida, H.; Watanabe, H.; Adachi, K.; Kotaka, T. *Macromolecules* **1991**, *24*, 2981.
(38) For a recent review see: Ngai, K. L. *J. Non-Cryst. Solids* **2000**, *275*, 7.
(39) Williams, G.; Watts, D. C. *Trans. Faraday Soc.* **1970**, *66*, 80.
(40) Richert, R.; Angell, C. A. *J. Chem. Phys.* **1998**, *108*, 9016.
(41) Adachi, K.; Kotaka, T. *Macromolecules* **1985**, *18*, 466.
(42) Imanishi, Y.; Adachi. K.; Kotaka, T. *J. Chem. Phys.* **1988**, *89*, 7585.
(43) Pakula, T.; Geyler, S.; Edling, T.; Boese, D. *Rheol. Acta* **1996**, *35*, 1.
(44) McLeish, T. C. B.; Milner, S. T. *Adv. Polym. Sci.* **1999**, *145*, 195.
(45) Matsumiya, Y.; Watanabe, H.; Osaki, K. *Macromolecules* **2000**, *33*, 499.
(46) Graessley, W. W. *Adv. Polym. Sci.* **1974**, *16*, 1.
(47) Stockmayer, W. H.; Burke, J. J. *Macromolecules* **1969**, *2*, 647.

MA020293B